Non-standard Timoshenko beam model for chiral metamaterial: identification of stiffness parameters

Michele De Angelo^{a,b}, Luca Placidi^d, Nima Nejadsadeghi^c, Anil Misra^{b,*}

Abstract

In the literature of granular micromechanics it is standard to achieve, at the macro scale, non-standard enhanced continuum models [1-2]. Among a panoply of exotic behaviors, these models predict that granular materials can show chirality for a specific grain-pair interaction. To verify these predictions, a granular system with a specific grain-pair interaction has been designed and its mechanical behavior under different types of loading has been evaluated via numerical simulations. The resulting granular system, which can be referred to as a granular beam, is a linear array of grains connected via the chosen grain-pair interaction law [1]. The chiral behavior of such mechanical system has been observed experimentally during tensile test. To describe the experimental evidence and numerical results, a continuous one-dimensional beam model has been defined and the four constitutive parameters, which characterize this specific strain energy function, have been identified. The numerical simulations on this granular system, modeled as a 2D deformable-body, have been performed employing the commercial finite element software COMSOL Multiphysics to have a reference data set for the identification process. Comparisons between the results obtained from this 2D FE model and the predictions of the same system analyzed via a specific non standard Timoshenko 1D beam model show an astonishing agreement.

Keywords: Granular Micromechanics, Enhanced Beam Model, Chiral Metamaterials

1. Introduction

In the field of material science, the study of mechanical behavior of materials and definition of suitable mathematical models faithfully representing reality is still of inter- 25 est. Specifically, we refer to the field of metamaterials -materials for which the microstructure present at a microscopic level has a non-negligible impact on macroscopic mechanical behavior- whose analysis has been facilitated by the continuous progress of additive manufacturing and 30 measuring techniques. The research is driven by the evidence that classical continuum models are not sufficient when we consider microstructured materials. One significant example is granular solids. Indeed, a non-standard enhanced continuum model based upon granular microme-35 chanics approach is required for representing the grainscale deformation modes [2, 3, 4]. At the spatial scale in which the continuum description is generally defined, the individual grain motion along with the grain-pair interaction is latent. However, in all their forms, whether highly 40 consolidated dense solids or soft cellular membranes or

Email address: amisra@ku.edu (Anil Misra)

^a Dipartimento di Ingegneria Civile, Edile-Architettura e Ambientale, Università degli Studi dell'Aquila, Via Giovanni Gronchi 18 - Zona industriale di Pile, 67100 L'Aquila, Italy.

^b Civil, Environmental and Architectural Engineering Department, The University of Kansas, 1530 W. 15th Street, Lawrence, KS 66045-7609. USA

^c Mechanical Engineering Department, University of Kansas, 1530 W. 15th Street, Learned Hall, Lawrence, KS 66045-7609, USA d'International Telematic University Uninettuno, C. so Vittorio Emanuele II 39, 00186 Rome, Italy

confined packings of non-cohesive particles, the grain pair interactions play a paramount role in determining physical behavior of granular media. Further example is represented by pantographic structures [5, 6, 7, 8, 9, 10], for which their exotic behavior has to be described with higher gradient continuum theories [11] or micromorphic theories [12, 13]. Lastly, we remark that granular system presented herein shares some key features with tensegrity cell mechanical metamaterial as axially loaded one-dimensional structures that have a broad literature on their dynamic behavior and their applications as energy absorption components [14, 15, 16]. The new manufacturing possibilities propel research to the point of reversing the paradigm used to date in studying the mechanical behavior of materials. We are now able to endow them with a micro-structure, which is potentially customizable and tunable according to the applications to be addressed. Therefore, once the system's Lagrangian has been defined, more precisely once the expression of the deformation energy density of the system has been expressed in term of the chosen independent kinematic parameters, we can design the corresponding mechanical system [17]. In the present work, we have considered a one-dimensional micropolar system with chirality

 $^{^* \\} Corresponding \ author$

which derives from a full understanding of the granular micromechanics model [1]. The geometric structure is a linear array of grains, which will be referred to as grain beam, whose grains are connected by a particular grain-pair connection. The design of the interaction is such that the axial displacement field is coupled with the transverse displacement field, that yields to a chiral macroscopic behavior of the grain beam. A modified Timoshenko beam model is defined to fulfill a micro-macro identification of the structure. The work developed in this article demonstrates common tracts with mechanical cable models in which the axial and twist mechanical behaviors are coupled, which could have relevant impact in the field of manufactured rope and cables or the analysis of DNA filaments [18, 19, 20]. The identification aims at determining the stiffness parameters which characterize the strain energy function of the modified Timoshenko beam model. We have accounted as reference data set the results obtained from a series of numerical simulation performed with the commercial Finite Element software Comsol Multiphysics. Specifically, different sets of boundary conditions have been applied to the granular structure which has been considered as a 2D Cauchy deformable-body.

2. Beam model

Let us consider a curve C in reference plane xy lying on the x axis in the undeformed configuration. The current configuration C' of the curve is given by the map χ which depends on the generic x_0 coordinate as shown in Fig. 1a. The analytical beam model that we are introducing describes the configuration of the granular system, which is characterized by the kinematic variables shown in Fig. 1b. Thus, we define the vector χ as

$$\chi(x) = \{w(x), u(x), \theta(x)\}^T \tag{1}$$

whose components $w(x), u(x), \theta(x)$ correspond to the axial displacement, transverse displacement and rotation of the grains respectively. We now consider the following expression of elastic deformation energy density, based on the kinematic parameters introduced

$$\mathcal{W} = \frac{1}{2} \mathbb{K}_{e} w'^{2} + \frac{1}{2} \mathbb{K}_{f} \theta'^{2} + \frac{1}{2} \mathbb{K}_{s} (u' - \theta)^{2} - \alpha w' (u' - \theta). \quad (2)_{80}$$

Eq.(2) resembles a classical Timoshenko beam with an additional term appearing in the expression. The stiffness coefficient α couples, using the classical terms of beam theories, the axial deformation measure w' with the shear 85 deformation measure $(u' - \theta)$. Rewriting Eq.(2) in matrix form it can be noted that the stiffness matrix is no more diagonal:

$$\mathcal{W} = \frac{1}{2} \begin{bmatrix} w' & u' - \theta & \theta' \end{bmatrix} \begin{bmatrix} \mathbb{K}_e & \alpha & 0 \\ \alpha & \mathbb{K}_s & 0 \\ 0 & 0 & \mathbb{K}_f \end{bmatrix} \begin{bmatrix} w' \\ u' - \theta \\ \theta' \end{bmatrix}$$

Moreover, the stiffness parameters must fulfill the following conditions which ensure that the stiffness matrix is positive definite

$$\mathbb{K}_e \mathbb{K}_s > \alpha^2; \quad \mathbb{K}_f > 0$$
 (3)

The system of differential equations and boundary condi-

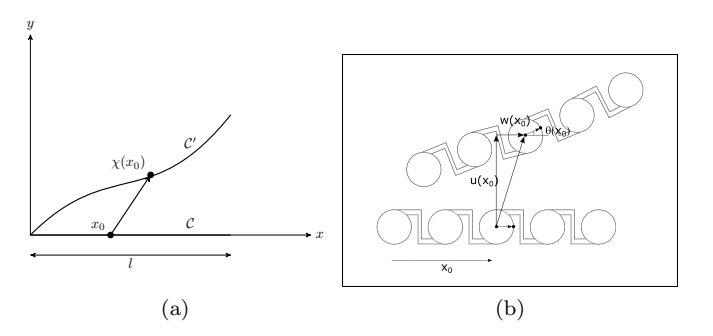


Figure 1: (a) Generic deformed configuration of the beam model in the reference plane xy (b) graphic description of the kinematic fields w(x), u(x) and $\theta(x)$.

tions have been obtained for the present beam model by imposing the first variation of the strain energy functional to be equal to 0.

$$\begin{cases} \mathbb{K}_{e}w'' - \alpha (u'' - \theta') = 0 \\ \mathbb{K}_{s} (u'' - \theta') - \alpha w'' = 0 \\ \mathbb{K}_{f}\theta'' - \alpha w' + \mathbb{K}_{s} (u' - \theta) = 0 \end{cases}$$
(4.a)
$$(4.b)$$

$$(4.c)$$

$$\mathbb{K}_f \theta'' - \alpha w' + \mathbb{K}_s (u' - \theta) = 0$$
 (4.c)

$$\begin{cases} \left[\mathbb{K}_{e}w' - \alpha \left(u' - \theta\right)\right] \delta w = 0 & \text{at } x=0, x=L \\ \left[\mathbb{K}_{s} \left(u' - \theta\right) - \alpha w'\right] \delta u = 0 & \text{at } x=0, x=L \\ \left[\mathbb{K}_{f}\theta'\right] \delta \theta = 0 & \text{at } x=0, x=L \end{cases}$$
 (5.a)

We report the governing differential equations of the classical Timoshenko beam model in Eq. 6.a-6.b

$$\begin{cases} \frac{d}{dx}GAK_s\left(\tilde{u}'-\tilde{\theta}\right) = 0 & (6.a) \\ \frac{d}{dx}\left(EI\tilde{\theta}'\right) - GAK_s\left(\tilde{u}'-\tilde{\theta}\right) = 0 & (6.b) \end{cases}$$

where \tilde{u} , $\tilde{\theta}$, AGK_s and EI represent the classic kinematic variables and stiffness parameters of Timoshenko beam [21]. It is remarkable that the coupled system of differential equations of the derived model includes one additional equation (Eq. 4.a). The latter comes from the accounting of the longitudinal displacement w, which in the classical Timoshenko model could be considered as an separate problem. Further, the classical Timoshenko beam equations (Eq. 6.a-6.b) are enhanced with additional coupling terms which appear in Eq. 4.b-4.c.

Finally, we can identify from Eq. 5, the normal force N(x), the shear force T(x) and the bending moment M(x) of the 1D beam as:

$$N(x) = \mathbb{K}_e w' - \alpha \left(u' - \theta \right) \tag{7}$$

$$T(x) = \mathbb{K}_s (u' - \theta) - \alpha w' \tag{8}$$

$$M(x) = \mathbb{K}_f \theta' \tag{9}$$

We report the expressions of shear force and bending moment of the classical Timoshenko beam model in Eq. 10-11

$$\tilde{T}(x) = GAK_s \left(\tilde{u}' - \tilde{\theta} \right) \tag{10}$$

$$\tilde{M}(x) = EI\tilde{\theta}' \tag{11}$$

and it can be remarked that while the bending moment has identical expression an additional terms appears in the shear expression. Moreover, the equation Eq. 7 which express the normal force in the 1D beam model, has a different expression with respect to the classical bar model because an additional term due to the coupling appears.

3. Numerical simulations and stiff-¹³⁰ nesses identification

A numerical technique is developed to identify the stiffness values which characterize the energy density of the novel₁₃₅ beam model. The reference data set utilized to identify \mathbb{K}_e , \mathbb{K}_f , \mathbb{K}_s and α has been obtained by performing numerical simulation with the commercial finite element software COMSOL Multiphysics in which the granular system shown in Fig. 3 has been designed as a 2D deformable continuum and subjected to different cases of boundary conditions. The geometrical parameters of the grain-pair connection are depicted in Fig. 2 and their numerical values are listed in Table 1. The whole array used in the

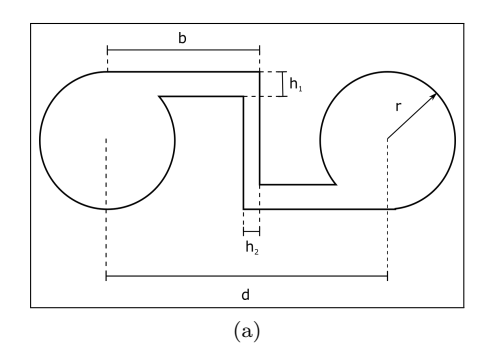


Figure 2: Graphic visualization of the geometric features of the grain pair connection.

simulation accounts for n=30 grains, being the total length l=0.435 m. We have considered three different type of planar equilibrium problems, which depending on the load direction and boundary conditions activate a subset of the stiffnesses defined in the energy density equation

Table 1: Values of geometric features of the grain-pair connection. Lengths are expressed in millimeters.

b	h_1	h_2	r	d
8.05	1.5	1.1	3.5	15

of Eq. (2). In Fig. 4 a graphic representation of the tests employed to accomplish the identification are shown. The realization of these simulations on the 2D granular system has been performed by considering the left and right boundary grains as rigid domains. The three degrees of freedom of the left rigid domain have been imposed equal to zero while the right grain has been displaced of $\delta = 0.001l$ and rotated by an angle $\mu = 0.001$ rad with respect his centroid, for Identification Test 1 and Identification Test 2, respectively. Differently, for Identification Test 3, zero horizontal and vertical displacement has been prescribed for both left and right grain, and a rigid rotation around each centroids has been imposed, with the angle $\mu = -0.001$ rad and $\mu = 0.001$ for the left and right rigid domain respectively. In Table 2 we report the corresponding analytical expression of the boundary conditions imposed on the 1D beam model, with $\delta = 0.001l$ and $\mu = 0.001$ rad. The deformed shape of the 2D granular system is shown in Fig. 5 for the three identification tests. As a result of the peculiar grain pair interaction, the system presents a vertical displacement when an axial displacement is prescribed (Fig. 5a). We remark that the coupling effect is independent of the size of the grain array and similar results are obtained for systems with different numbers of grains. In Fig. 6 the vertical components of the grain displacements under a load as Identification Test 1 is shown for different system sizes. The plots in Fig. 6a,b,c refer to a 10-grain system, a 20-grain system and a 30grain system, respectively. Overall, the displacements of the grains result to have comparable shapes with different amplitude, which has been amplified $2 \cdot 10^3$ times to facilitate visualization. Moreover, the chirality of the system is evident: if we performed reflection with respect to a plane parallel to the one on which the granular assembly lies by means of an orthogonal matrix with determinant equal to -1, we would obtain equal deformed shapes but opposite in sign, for all the identification tests.

Table 2: Analytical expression of boundary conditions of the Identification Tests.

Identification Test 1	Identification Test 2	Identification Test 3
w(0) = 0	w(0) = w(L) = 0	w(0) = w(L) = 0
u(0) = u(L) = 0	u(0) = u(L) = 0	u(0) = u(L) = 0
$\theta(0) = \theta(L) = 0$	$\theta(0) = 0$	$\theta(0) = -\mu$
$w(L) = \delta$	$\theta(L) = \mu$	$\theta(L) = \mu$

In the following procedure, a subset of the constitutive parameters have been estimated comparing the expression

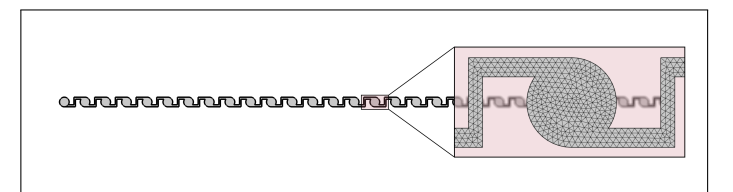


Figure 3: Granular system microstructure employed for the numerical simulation treating the system as a Cauchy continuum which is solved using full FE discretization. In the magnifying frame we show the mesh size for which the convergence is accomplished (the number of DOF is equal to 89718). The discretization is realized via triangular bi-dimensional elements whose displacement fields are approximated using quadratic serendipity polynomials.

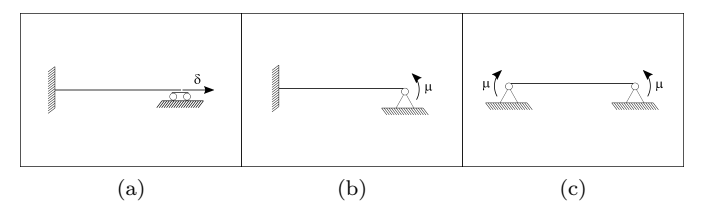


Figure 4: Graphic description of the boundary condition sets for (a) Identification Test 1, (b) Identification Test 2 and (c) Identification Test 3.

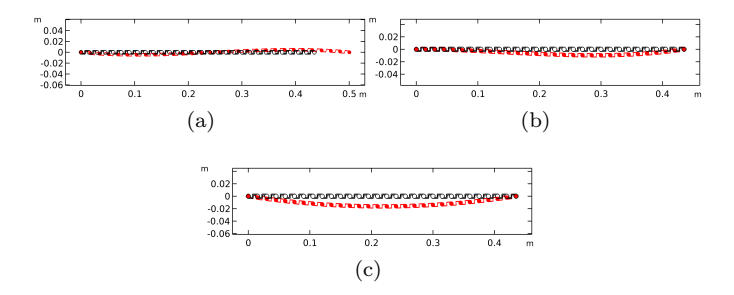


Figure 5: Deformed shapes of Cauchy continuum model of the 2D granular system for (a) Identification Test 1, (b) Identification Test 2 and (c) Identification Test 3.

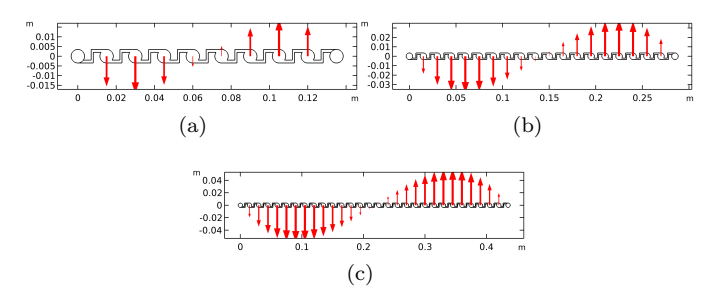


Figure 6: Vertical displacement of the 2D granular system for Identification Test 1. The red arrows represent the motion amplitude amplified of $2\cdot 10^3$ times for each grain, being the total number (a) 10 grains, (b) 20 grains, (c) 30 grains.

of total strain energy of the beam model

$$\mathcal{E}_i = \int_0^l \mathcal{W}(x) dx \tag{12}$$

with the total strain energy obtained with the 2D granular system. The index i will indicate the identification test to which the energy expression corresponds. The first stiffness parameter taken into account was the bending stiffness \mathbb{K}_f . By imposing the set of boundary conditions of Identification Test 3 (i=ID3), the expression of strain energy of 1D beam is

$$\mathcal{E}_{ID3} = \frac{2\mathbb{K}_f \mu^2}{l}.\tag{13}$$

We have evaluated the strain energy value from the FE calculation of the analogous case, and the bending stiffness of the 1D model have been calculated. The stiffness parameter \mathbb{K}_s has been identified by applying the boundary condition of the Identification Test 2 (i=ID2), which leads to the following expression for the strain energy

$$\mathcal{E}_{ID2} = \frac{2\mathbb{K}_f (36\mathbb{K}_f^2 l + 3\mathbb{K}_f \mathbb{K}_s l^3 + \mathbb{K}_s^2 l^5)\mu^2}{(-12\mathbb{K}_f l + \mathbb{K}_s l^3)^2}.$$
 (14)

By equalizing Eq. (14) with the strain energy value evaluated via the 2D numerical simulation, two possible solutions for \mathbb{K}_s were obtained. A quantitative comparison with the reference numerical simulation of the 2D granular system allowed to estimate the correct value of \mathbb{K}_s . In Fig. 7 the field u(x) of the beam model has been plotted for the two values obtained, which we have indicated with \mathbb{K}_{s1} and \mathbb{K}_{s2} . As depicted in Fig. 7, only one of the two values results in perfect agreement with the plot of transverse displacement of 2D granular system. Finally,

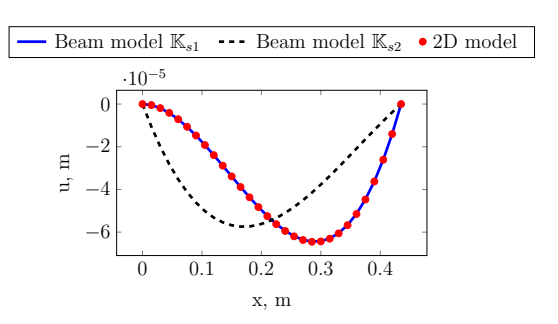


Figure 7: Transverse displacement u(x) of the beam model for \mathbb{K}_{s1} and \mathbb{K}_{s2} , and transverse displacement of 2D granular system, for Identification Test 3.

the Identification Test 1 allowed to evaluate stiffnesses \mathbb{K}_e and α . The latter has been found to be strictly related to the amplitude of the transverse motion under extension. For the current Identification Test 1, the area A(x) that the curve u(x) subtends with the x-axis has the following

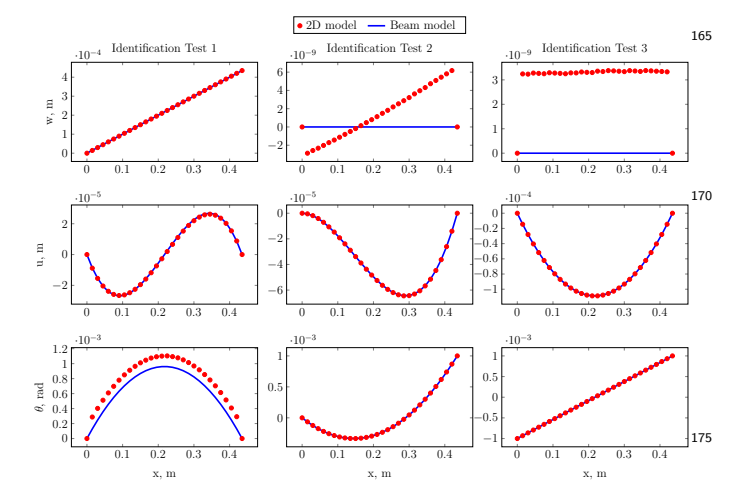


Figure 8: Comparison of kinematic fields between 2D granular system and the analytical beam model. The plots refer to Identification Tests of Table 2.

analytical expression:

$$A(x)_{ID1} = \frac{(l-x)^2 x^2 \alpha \delta}{24 \mathbb{K}_f + 2 \mathbb{K}_s l^3}$$
 (15)

The value of Eq. (15) at $x = \frac{l}{2}$ has been compared with the respective values obtained from the Cauchy bidimensional continuum model, and we have evaluated the stiffness parameter α . The extensional stiffness \mathbb{K}_e has been calculated via a comparison between the strain energy of the analytical beam model, which has the following expression

$$\mathcal{E}_{ID1} = \frac{\left(12\mathbb{K}_e \mathbb{K}_f + \mathbb{K}_e \mathbb{K}_s l^2 + 3l^2 \alpha^2\right) \delta^2}{24\mathbb{K}_f l + 2\mathbb{K}_s l^3}$$
(16)₁₈₅

and 2D continuum model. The final set of constitutive parameters of the beam model are reported in Table 3. A first verification of the identified value is reported in

Table 3: Stiffness values after identification process.

$\mathbb{K}_{e}\left[N ight]$	$\mathbb{K}_{s}\left[N ight]$	$\mathbb{K}_f\left[N\cdot m^2 ight]$	$\alpha \left[N \right]$
49545.4243	18819.4046	0.3307	-12048.7

Fig. 8. Considering the stiffness values of Table 3, we have evaluated the kinematic fields w(x), u(x) and $\theta(x)$ of the beam model for Identification Test 1, Identification Test 2 and Identification Test 3. The plots have been compared with the corresponding values obtained from the 2D numerical simulations for the three tests. In each plot of Fig. 8, the solid line represents the components of the vector χ while the points represent the plane displacement components and the rotation of each grain. It can be observed that a precise overlap of results occurs except in one case. The grain rotation of the 2D model has somewhat higher

values with respect to the field $\theta(x)$ of the beam model, for Identification Test 1. It is noted that the apparent mismatch between plots of the axial displacement w(x) of the two models for Identification Tests 2 and 3 is negligible as the order of magnitude 10^{-9} is insignificant compared to other kinematic quantities.

4. Validation

In order to prove the actual forecasting capability of the identified beam model toward the 2D granular system, we compare the two for four independent tests different from the ones used for the identification. A graphic representation of boundary conditions of validation tests is shown in Fig. 9. The realization of numerical simulations for the 2D granular system has been performed by considering the boundary grains as rigid domains. The left grain has been considered fixed for all the simulations, while on the right grain, the boundary conditions are listed in Table 4. In

Table 4: Prescribed displacements and rotations on the right grain of 2D granular system for Validation Tests.

	horizontal disp.	transverse disp	rotation
Val. Test 1	$\delta = -0.001l$	0	0
Val. Test 2	$\delta = -0.001l$	$\delta = 0.001l$	0
Val. Test 3	0	$\delta = 0.001l$	$\mu=0.001~\rm rad$
Val. Test 4	$\delta = -0.001l$	$\delta = 0.001l$	$\mu=0.001~\rm rad$

Table 5 we give the respective analytical expressions of boundary conditions applied to 1D beam model. The deformation of the 2D continuum model of the granular system has been evaluated for all the above mentioned sets of boundary loads, and each deformed shape is shown in Fig. 9. Similarly, we have evaluated the deformed configuration

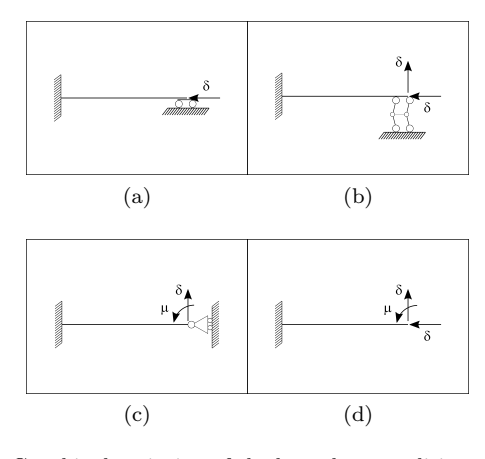


Figure 9: Graphic description of the boundary condition sets for (a) Validation Test 1 (b) Validation Test 2 (c) Validation Test 3 (d) Validation Test 4

of the beam model employing the identified values of the

constitutive parameters \mathbb{K}_e , \mathbb{K}_s , \mathbb{K}_f , α for the 4 load cases of Table 5, and the values of the kinematic fields w(x), u(x) and $\theta(x)$ were compared with the results obtained from simulations of 2D model under the same loading conditions. The plots for Validation Test 1 are shown in the first column of Fig. 10, and they reveal a good agreement between the 1D beam model and the reference data. It is noticeable that when the beam undergoes a compression of a small amount, a non negligible vertical displacement field u(x) and a rotation field $\theta(x)$ arise. Moreover, comparing the plots of the kinematic fields between Identification Test 1 (see Fig. 8) and Validation Test 1 (see Fig. 10), a precise symmetry with respect to the x-axis can be observed. Lastly, it is evident that the behavior of the present 1D beam model is different with respect to a standard Timoshenko beam model undergoing identical boundary conditions. The comparison between kinematic fields of 1D beam model and 2D granular system for Validation Test 2 are reported in the second column of Fig. 10. An adequate agreement can be noted for the axial and transverse displacements, but for the rotation field $\theta(x)$ a slight dissimilarity occurs. This aspect, which must be investigated more in future works, can be related to a boundary effect on the rotation of external grains of the 2D granular system. The third column of Fig. 10 shows the displacement fields of 1D beam model and 2D granular system for Validation Test 3. A careful overlap can be observed for the transverse displacement u(x) and the rotation $\theta(x)$. However, a discrepancy is present between the kinematic field w(x) and the axial displacement of the 245 grains, but the relative error committed is negligible at a length-scale of the field u(x) and the vertical displacement of the grain assembly. We have to remark that, the displacement fields of 1D beam model produced by Validation Test 2 and 3 have similar behaviors compared to²⁵⁰ those provided by a classical Timoshenko beam model under respectively identical boundary conditions. The fourth column of Fig. 10 reports the plots of displacement field of 1D beam model and the displacements of the 2D granular system for Validation Test 4. It can be observed that 255 the beam model faithfully describes the behavior of the 2D granular system in all the three components. As for Validation Test 1 a Timoshenko beam model under a set of boundary conditions as Validation Test 4 gives different behaviors for transverse displacement u(x) and rotation²⁶⁰ field $\theta(x)$.

5. Conclusions and perspective

One of the most recurrent themes in the literature of continuous mechanics is the formulation of reduced models for describing structures and mechanical systems. Reducing the size of the variables with which a physical system is described has the immediate advantage of facilitating calculations and reducing their computation time. On the other hand, the information we can access will be less ac-

Table 5: Analytical expression of boundary conditions of the Validation Tests

Val. Test 1	Val. Test 2	Val. Test 3	Val. Test 4
w(0) = 0	w(0) = 0	w(0) = w(l) = 0	w(0) = u(0) = 0
u(0)=u(l)=0	u(0) = 0	u(0) = 0	$\theta(0) = 0$
$\theta(0) = \theta(l) = 0$	$\theta(0) = \theta(l) = 0$	$\theta(0) = 0$	$\theta(l) = \mu$
$w(l) = -\delta$	$w(l) = -\delta$	$\theta(l) = \mu$	$w(l) = -\delta$
	$u(l) = \delta$	$u(l) = \delta$	$u(l) = \delta$

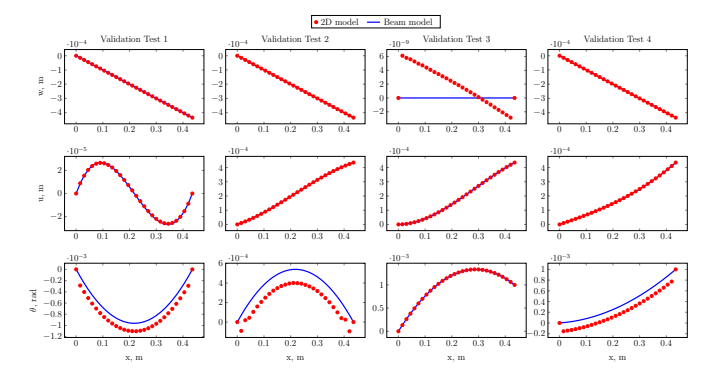


Figure 10: Comparison of kinematic fields between 2D granular system and the analytical beam model. The plots refer to Validation Tests of Table 5.

curate. As a remark, the transition from a refined model to a reduced order one is necessary when we are dealing with complex systems [22, 23, 24, 25, 26, 27]. In this paper, we have presented an identification process of constitutive parameters that characterize the deformation energy density of a chiral beam model. This model can be considered as an enhanced model of the Timoshenko beam with an additional stiffness term that couples the horizontal and transverse displacement fields of the beam. As a result of this coupling, chiral behavior is triggered. The identification process has considered as a reference data set the results of numerical simulations employing a 2D Cauchy continuum in which a linear assembly of grains has peculiar granular interaction. The design of the grain-pair connection has been inspired by the study on the constitutive relations formulated for granular materials following granular micromechanics approach [1]. The identification has been proven to be effective via validation tests in which we have observed perfect agreement between the results of the enhanced Timoshenko beam model and reference data. Despite the results obtained, the present work represents the first step toward a complete analysis of the introduced micropolar granular system with chirality. A thorough experimental survey seems necessary to (a) establish the chiral behavior for a larger set of specimens and (b) to obtain a consistent reference data set for future identification processes. Moreover, the dynamics of microstructured materials and their mechanical response towards time-varying loads and waves propagation is a crucial point. In the wake of earliest study investigating dynamics of granular

system [28, 29, 30] and pantographic structures [31, 32, 33], it is particularly useful to have both predictive continuum models as well as innovative experimental evidence.

Acknowledgement

This work was supported in part by the United States National Science Foundation (grant CMMI-1727433).

References

320

335

- A. Misra, N. Nejadsadeghi, M. De Angelo, L. Placidi, Chiral metamaterial predicted by granular micromechanics: Verified with 1d example synthesized using additive manufacturing, under review.
 - [2] A. Misra, P. Poorsolhjouy, Grain-and macro-scale kinematics for³⁵⁵ granular micromechanics based small deformation micromorphic continuum model, Mechanics Research Communications 81 (2017) 1–6.
 - [3] A. Misra, P. Poorsolhjouy, Granular micromechanics based micromorphic model predicts frequency band gaps, Continuum³⁶⁰ Mechanics and Thermodynamics 28 (1-2) (2016) 215–234.
 - [4] P. Poorsolhjouy, A. Misra, Granular micromechanics based continuum model for grain rotations and grain rotation waves, Journal of the Mechanics and Physics of Solids 129 (2019) 244–260.
- [5] F. dellIsola, P. Seppecher, J. J. Alibert, T. Lekszycki, R. Grygoruk, M. Pawlikowski, D. Steigmann, I. Giorgio, U. Andreaus, E. Turco, et al., Pantographic metamaterials: an example of mathematically driven design and of its technological challenges, Continuum Mechanics and Thermodynamics (2018) 1–370 34.
- [6] A. Misra, T. Lekszycki, I. Giorgio, G. Ganzosch, W. H. Müller, F. Dell'Isola, Pantographic metamaterials show atypical poynting effect reversal, Mechanics Research Communications 89 (2018) 6–10.
- [7] F. 'Isola, T. Lekszycki, M. Pawlikowski, R. Grygoruk, L. Greco, Designing a light fabric metamaterial being highly macroscopically tough under directional extension: first experimental evidence, Zeitschrift für angewandte Mathematik und Physik 66 (2015) 3473–3498.
 - [8] I. Giorgio, N. Rizzi, E. Turco, Continuum moing of pantographic sheets for out-of-plane bifurcation and vibrational analysis, Proc. R. Soc. A 473 (2207) (2017) 20170636.
 - [9] I. Giorgio, A. Della Corte, F. dell'Isola, Dynamics of 1d nonlinear pantographic continua, Nonlinear Dynamics 88 (1) (2017)³⁸⁵ 21–31.
 - [10] F. dell'Isola, I. Giorgio, M. Pawlikowski, N. Rizzi, Large deformations of planar extensible beams and pantographic lattices: heuristic homogenization, experimental and numerical examples of equilibrium, in: Proc. R. Soc. A, Vol. 472, The Royal Society,³⁹⁰ 2016, p. 20150790.
 - [11] N. Auffray, F. dell'Isola, V. Eremeyev, A. Madeo, G. Rosi, Analytical continuum mechanics à la Hamilton-Piola least action principle for second gradient continua and capillary fluids, Mathematics and Mechanics of Solids 20 (4) (2015) 375–417.
- [12] W. Pietraszkiewicz, V. Eremeyev, On natural strain measures of the non-linear micropolar continuum, International Journal of Solids and Structures 46 (3) (2009) 774–787.
 - [13] H. Altenbach, V. Eremeyev, On the linear theory of micropolar plates, ZAMM-Journal of Applied Mathematics and Me-400 chanics/Zeitschrift für Angewandte Mathematik und Mechanik 89 (4) (2009) 242–256.
 - [14] A. Amendola, E. Hernández-Nava, R. Goodall, I. Todd, R. Skelton, F. Fraternali, On the additive manufacturing, post-tensioning and testing of bi-material tensegrity structures, Composite Structures 131 (2015) 66–71.

- [15] R. Goyal, R. E. Skelton, Tensegrity system dynamics with rigid bars and massive strings, Multibody System Dynamics 46 (3) (2019) 203–228.
- [16] Q. Zhang, D. Zhang, Y. Dobah, F. Scarpa, F. Fraternali, R. E. Skelton, Tensegrity cell mechanical metamaterial with metal rubber, Applied Physics Letters 113 (3) (2018) 031906.
- [17] J.-J. Alibert, P. Seppecher, F. dell'Isola, Truss modular beams with deformation energy depending on higher displacement gradients, Mathematics and Mechanics of Solids 8 (1) (2003) 51–73.
- [18] T. Healey, Material symmetry and chirality in nonlinearly elastic rods, Mathematics and Mechanics of Solids 7 (4) (2002) 405–420
- [19] G. A. Costello, Theory of wire rope, Springer Science & Business Media, 1997.
- [20] C. R. Calladine, H. Drew, Understanding DNA: the molecule and how it works, Academic press, 1997.
- [21] J. N. Reddy, An introduction to the finite element method (1989).
- [22] E. Barchiesi, F. DellIsola, M. Laudato, L. Placidi, P. Seppecher, A 1d continuum model for beams with pantographic microstructure: Asymptotic micro-macro identification and numerical results, in: Advances in Mechanics of Microstructured Media and Structures, Springer, 2018, pp. 43–74.
- [23] M. De Angelo, E. Barchiesi, I. Giorgio, B. E. Abali, Numerical identification of constitutive parameters in reduced-order bi-dimensional models for pantographic structures: application to out-of-plane buckling, Archive of Applied Mechanics (2019) 1–26.
- [24] E. Barchiesi, S. Khakalo, Variational asymptotic homogenization of beam-like square lattice structures, Mathematics and Mechanics of Solids (2019) 1081286519843155.
- [25] L. Placidi, G. Rosi, E. Barchiesi, Analytical solutions of 2dimensional second gradient linear elasticity for continua with cubic-d 4 microstructure, in: New Achievements in Continuum Mechanics and Thermodynamics, Springer, 2019, pp. 383–401.
- [26] E. Turco, I. Giorgio, A. Misra, F. DellIsola, King post truss as a motif for internal structure of (meta) material with controlled elastic properties, Royal Society open science 4 (10) (2017) 171153.
- [27] I. Giorgio, P. Harrison, F. Dell'Isola, J. Alsayednoor, E. Turco, Wrinkling in engineering fabrics: a comparison between two different comprehensive modelling approaches, Proceedings of the Royal Society A: Mathematical, Physical and Engineering Sciences 474 (2216) (2018) 20180063.
- [28] N. Nejadsadeghi, A. Misra, Axially moving materials with granular microstructure, International Journal of Mechanical Sciences 161 (2019) 105042.
- [29] N. Nejadsadeghi, L. Placidi, M. Romeo, A. Misra, Frequency band gaps in dielectric granular metamaterials modulated by electric field, Mechanics Research Communications 95 (2019) 96–103.
- [30] A. Misra, N. Nejadsadeghi, Longitudinal and transverse elastic waves in 1d granular materials modeled as micromorphic continua, Wave Motion 90 (2019) 175–195.
- [31] M. Laudato, L. Manzari, E. Barchiesi, F. Di Cosmo, P. Göransson, First experimental observation of the dynamical behavior of a pantographic metamaterial, Mechanics Research Communications 94 (2018) 125–127.
- [32] E. Barchiesi, M. Laudato, F. Di Cosmo, Wave dispersion in non-linear pantographic beams, Mechanics Research Communications 94 (2018) 128–132.
- [33] F. dellIsola, P. Seppecher, M. Spagnuolo, E. Barchiesi, F. Hild, T. Lekszycki, I. Giorgio, L. Placidi, U. Andreaus, M. Cuomo, et al., Advances in pantographic structures: design, manufacturing, models, experiments and image analyses, Continuum Mechanics and Thermodynamics (2019) 1–52.